Received: 16 June 2018 | Revised: 3 December 2018 | Accepted: 10 January 2019

DOI: 10.1002/joc.5999

International Journal of Climatology RMetS

RESEARCH ARTICLE

ENSO teleconnections to the Indian summer monsoon under changing climate

Indrani Roy[1] | Renata G. Tedeschi[2] | Matthew Collins[1]

[1]College of Engineering, Mathematics and Physical Sciences, University of Exeter, Exeter, UK

[2]Centro de Previsão do Tempo e Estudos Climáticos, Instituto Nacional de Pesquisas Espaciais, São Paulo, Brazil

Correspondence
Indrani Roy, College of Engineering, Mathematics and Physical Sciences, University of Exeter, Exeter, UK.
Email: indrani_r@hotmail.com

The teleconnection between the El Niño–Southern Oscillation (ENSO) and Indian summer monsoon rainfall is analysed in CMIP5 simulations in both historical and future scenario. A subset of models is selected, based on their ability to simulate mean rainfall and the ENSO teleconnection in the historical simulations, and those are used to examine future predictions in the central northeast region of India. For canonical and mixed canonical Modoki ENSO events, the rainfall teleconnection is spatially extended over most of India in the future. For pure Modoki ENSO events, the teleconnection disappears, and practically no influence is detected in any parts of India. Analysis of zonal wind at 200 mb indicates that for the Modoki events, there is a larger spread of changes across the models, while for canonical events there is more inter-model consistency. A rainfall decomposition technique reveals a battle between changes in circulation which act to weaken the rainfall teleconnection and changes in moisture change which act to strengthen it. The picture is most consistent in the sub-ensemble of models in the central northeast region but less consistent in regions covering southern India.

KEYWORDS

canonical ENSO, CMIP5, Modoki ENSO, RCP8.5

1 | INTRODUCTION

The Indian summer monsoon (ISM) plays a very important part of India's socio-economic infrastructure as it receives about 80% of the total rainfall during this season. The Indian economy is dependent on agriculture and related industries and experiences profound impact due to the variability in the ISM. Hence, future prediction of potential changes in the ISM in terms of its regional response serves a crucial role not only to Indian economy but also has consequences for global wealth generation.

The El Niño–Southern Oscillation (ENSO), the most dominant tropospheric variability around tropical Pacific, is found to be strongly coupled with the ISM. Drought years in India are usually aligned with warm ENSO or El Niño years while excess rainfall years match with La Niña. Several studies have discussed ENSO–ISM teleconnections (Turner *et al*., 2005; Kumar *et al*., 2006; Roy, 2017); moreover, few studies also detected some complementary effect on the ISM from the Indian Ocean Dipole (Ashok *et al*., 2001) and also from the North Atlantic Oscillation (NAO) in the previous seasons (Liu and Yanai, 2001). Such connections were shown to be sensitive to the chosen reference period of the observations (Roy and Collins, 2015). Numerous studies also revealed the climate effect of the ENSO in other parts of the world, for example, North Atlantic and European sector (Lin and Wu, 2012).

It has become common to discuss two types of ENSO. One is dominated by variability of Sea Surface Temperature (SST) centred in the eastern tropical Pacific, commonly known as the East Pacific (EP) type or canonical ENSO and the other dominated by strong SST variability around the

central tropical Pacific, commonly known as central Pacific (CP) type or Modoki ENSO (Ashok *et al*., 2007). The teleconnection patterns associated with these two ENSO types indicate different impacts in various parts of the world (Brown *et al*., 2009; Cai and Cowan, 2009; Roy *et al*., 2017; Tedeschi and Collins, 2017; Roy, 2018). For example, Cai and Cowan (2009) studied La Niña Modoki influence on precipitation over Australia. They showed that precipitation during March–April–May increases, extending from northwestern Australia to the northern Murray-Darling Basin during La Niña Modoki. During a canonical La Niña, the region of increased precipitation shifts eastwards. The formation mechanism of these two types of ENSO is also found to be different; for the canonical case, the thermocline plays a dominant role, while for Modoki, zonal advection and midlatitude interactions are proposed as more important (Kao and Yu, 2009; Yu and Kim, 2011). Different solar decadal influence on the mechanisms of two types of ENSO is also recently explored by Roy and Kriplani (2018).

Another new type of ENSO, named the "mega-ENSO," has also been discussed (Wang *et al*., 2013; Wu and Zhang, 2015; Zhang *et al*., 2017). It has a pattern similar to the Inter-decadal Pacific Oscillation but involves both multidecadal and inter-annual SST variations. Mega-ENSO was shown to have a strong influence on the Northern Hemisphere summer monsoon (Wang *et al*., 2013), North Pacific atmospheric circulation in winter (Zhang *et al*., 2017) and winter NAO (Wu and Zhang, 2015). Many studies also explored other types of ENSO events and their impact on ISM rainfall. For example, Zhang *et al*. (2016) analysed different impacts of typical and atypical developing ENSOs on the Indian summer rainfall. The current study, however, focuses only on canonical and Modoki types of ENSO.

Various modelling groups around the world have coordinated climate model experiments known as Coupled Model Inter-comparison Project (CMIP5) (Taylor *et al*., 2012). These model simulations may be used to better understand the ENSO–ISM teleconnection during various types of ENSO events and changes under climate change (Jourdain *et al*., 2013; Roy and Tedeschi, 2016; Roy *et al*., 2017).

Changes in the ISM in future have been analysed (Zou and Zhou, 2015; Azad and Rajeevan, 2016) which suggest significant changes from the historical period. Azad and Rajeevan (2016) studied ISM and ENSO teleconnection in a future scenario analysing 20 different CMIP5 models and suggested a shift from a 3–5-year period band of variability in the historical period to shorter periods in future (2.5–3 year). Using four different Chinese models from the CMIP5 ensemble, Zou and Zhou (2015) showed that although the projected future climate changes over the Arabian Sea were the same among models, the associated mechanisms were quite different. The Arabian Sea plays an important role on delayed or advanced onset of the monsoon. However, there is a lack of understanding relating to how ISM–ENSO teleconnection will evolve in the future, especially when the focus is on the various sub-categories of ENSO. This study focuses on those areas.

The work of Cappondonti *et al*. (2015) nicely discussed the current state of understanding on ENSO diversity and identified major areas of gaps in knowledge. Studies indicated the importance of exploring the link between changes in ENSO and the mean state of the Pacific climate, to understand the varied nature of ENSO in future (Cai *et al*., 2015). Yeh *et al*. (2018) on the other hand discussed that future changes of ENSO teleconnection do not currently indicate strong agreement among models.

Various thermodynamic scaling arguments have been put forward to explain future changes in rainfall (Held and Soden, 2006). They include "warmer-get-wetter" (John *et al*., 2009; Xie *et al*., 2010) and "wet-get-wetter" (Chou *et al*., 2009). Recent studies indicate that changes in circulation are central (Seager *et al*., 2010; Chadwick *et al*., 2013; Huang *et al*., 2013) and hence it is appropriate to use techniques to decompose rainfall changes associated with both moisture and circulation. We employ such a technique to explain the changes in tropical rainfall under climate change considering the effect of both "dynamical" and "thermodynamical" part (Seager *et al*., 2012; Chung *et al*., 2014) including changes in the behaviour of ENSO–ISM teleconnection during differently flavours of ENSO (Huang *et al*., 2013; Huang, 2014; Huang and Xie, 2015).

The ISM represents a large-scale heat source on the equator around Intertropical Convergence Zone (ITCZ) covering central northeast (CNE) India. Following the linear theory, it is related to both the regional Hadley as well as the Walker circulation (Gill, 1980) and hence the main focus of this analysis is on CNE region. Earlier work studied extratropical ENSO teleconnections in CMIP5 models (Charlton-Perez, 2013; Hurwitz *et al*., 2014) separating models as high top (H) (H models have upper lids up to the Stratopause [1 hPa]) and low top (L). It is believed that high-top models with polar vortex feature may capture polar annular mode pattern better (Charlton-Perez, 2013; Osprey *et al*., 2013; Seviour *et* al., 2016). Moreover, studies identified an ISM–Southern Annular Mode (SAM) teleconnection in observations where Modoki ENSO plays the dominant role (Prabhu *et al*., 2016). Hence, initially we separate models with high and low tops to detect if it is possible to identify a subset of models performing better over the others.

2 | METHODOLOGY

Different regions of Pacific are defined as follows: canonical region (90°–140°W, 5°N–5°S), region A (165°E–140°W, 10°S–10°N), region B (110°–70°W, 15°S–5°N) and region C (125°–145°E, 10°S–20°N) and shown in Figure 1.

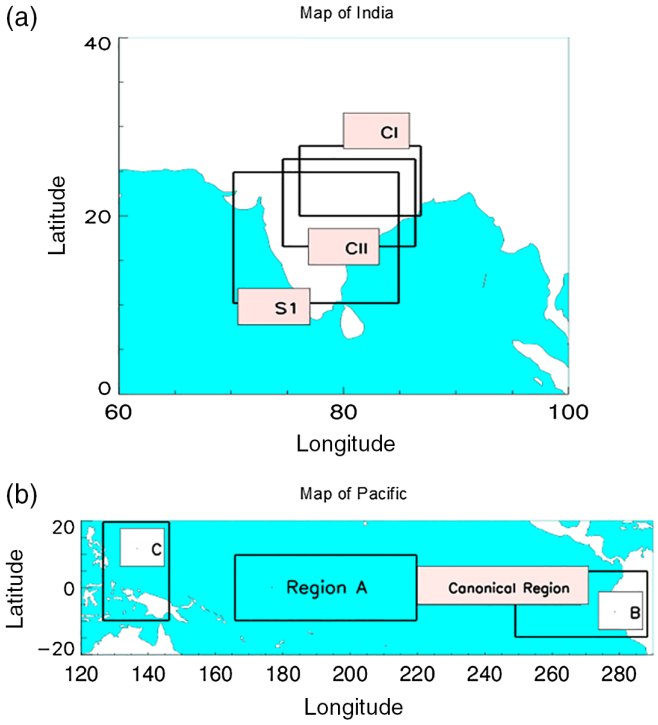

FIGURE 1 Map of India (a) showing CI, CII and S1 regions and the tropical Pacific (b) for defining different types of ISM rainfall and ENSO [Colour figure can be viewed at wileyonlinelibrary.com]

Various definitions for ENSO are used following SST anomalies (SSTAs) in those regions (Ashok *et al*., 2007; Kao and Yu, 2009; Kug *et al*., 2009; Tedeschi *et al*., 2013):

- ENSO Modoki Index (EMI):

EMI = (region A SSTA) − 0.5(region B SSTA) − 0.5 (region C SSTA).

- ENSO canonical (ENC/LNC): SSTA in the canonical region is greater/less than $0.7\sigma_C$, where σ_C is the standard deviation (*SD*) of SSTAs in that region.
- ENSO Modoki (ENM/LNM): if the EMI is greater/less than $0.7\sigma_M$, where σ_M is the *SD* of the EMI and region A SSTA is greater than $0.7\sigma_A$, σ_A is the *SD* of the region A SSTAs.
- Mixed ENSO canonical and Modoki (ENCM/LNCM): SSTAs fulfil both the canonical and Modoki conditions.

We remove the trend from data and initially applied correlation and compositing techniques. For the compositing analysis, the additional region A features in the definition of Modoki events (Ashok *et al*., 2007) are used (Tedeschi *et al*., 2013).

The level of significance for the correlation analysis is tested using Student's *t* test. For compositing, the hypergeometric test (Meyer, 1970; Ropelewski and Halpert, 1987) is applied which is also used in other studies (Grimm, 2004; Tedeschi *et al*., 2013).

A previous study (Bollasina *et al*., 2011), identified a box region in the CNE India (76°–87°E, 20°–28°N) that showed a significant decreasing trend in ISM rainfall during the later half of the last century. Extending that box to the east of the Peninsular (74.5°–86.5°E and 16.5°–26.5°N) also produces a similar trend (Goswami *et al*., 2006). Those two regions from the CNE are used here to discuss ISM–ENSO teleconnections and are shown as CI and CII in Figure 1. In addition to the CI and CII regions, a region from southern India S1 (70°–85°E and 10°–25°N) is also selected as it shows strong influences for canonical and canonical Modoki situation in the future (Figure 1).

A precipitation decomposition technique is also applied. Changes in tropical precipitation under climate change are linked to variations in circulation as well as moisture (Held and Soden, 2006; Huang *et al*., 2013; Huang, 2014). The decomposition of tropical precipitation (P) changes is adopted (Huang *et al*., 2013; Huang, 2014) as follows:

$$\Delta P \sim -(q \cdot \Delta\omega + \Delta q \cdot \omega), \quad (1)$$

where ω is the pressure velocity at 500 hPa and q is the surface specific humidity both at the historical period. Δ is the change between the historical and future scenario. This decomposition relationship can also be applied to examine the variability of tropical precipitation during different types of ENSO years (Huang and Xie, 2015):

$$\Delta P' \sim -\left(\Delta q \cdot \omega' + q \cdot \Delta\omega' + q' \cdot \Delta\omega \cdot \Delta q' \cdot \omega\right). \quad (2)$$

The prime indicates composite during different ENSO events, while the other notation is the same as Equation 1. We use Equation 2 to observe how variations in circulation and humidity under climate change influence various ENSO-related precipitation in India.

We analyse CMIP5 simulations from the historical period 1861–2005 (Taylor *et al*., 2012) and representative concentration pathways 8.5 situation (RCP8.5) (Riahi *et al*., 2011) from 2006 to 2095. A total of 35 most commonly used models were chosen and are listed in Table S1, Supporting Information. Some models only have one ensemble member, and hence for consistency, the first ensemble member from each of 35 models is analysed. All the observed data and model outputs are also interpolated onto a 1 × 1° latitude and longitude grid to maintain uniformity. Models are also separated as a high top (H) or low top (L) (Table S1). A group of eight models those reproduce the climatology of ISM rainfall over India well (Jourdain *et al*., 2013) are used for ensemble analyses and are marked as 1 to 8 [ACCESS1-0(1), CCSM4(2), CanESM2(3), FIO-ESM (4), HadGEM2-AO(5), HadGEM2-ES(6), MIROC5(7), NorESM1-ME(8)], also shown in Table S1.

For ISM precipitation, observational data from Global Precipitation Climatology Project (GPCP) is used (Huffman *et al*., 2009). This is monthly data available on a 2.5° grid from 1979 to the present. The combination of satellite-based rainfall estimates is the most complete analysis of rainfall

over the oceans with spatial detail to the rainfall over land. These data are available from NOAA/OAR/ESRL PSD, Boulder, CO (link: http://www.esrl.noaa.gov/psd/). SST data are from Met Office Hadley Centre Sea Ice and Sea Surface Temperature (HadISST) data (Rayner *et al*., 2003) and are monthly globally complete fields of SST and sea ice concentration on a 1° grid. These data are also available from NCAS British Atmospheric Data Centre (http://badc.nerc.ac.uk/view/badc.nerc.ac.uk_ATOM_dataent_hadisst).

3 | RESULTS

3.1 | Comparing ISM during historical periods with observation using Taylor diagram

Using Taylor diagrams (Taylor, 2001), we assess model performance against observations (Figure 2) in regions CI and CII. Such analyses help to identify better performing models, which may be more useful than others for future prediction purposes. We focus on the precipitation climatology. Models with negative pattern correlations are identified and separated from those showing positive correlation and placed in separate diagrams. Models which are closer to the observed *SD*, along with higher correlation values and hence lesser RMS errors are designated the better performing models (Taylor, 2001). Names of models with chosen ID, pattern correlation coefficient (only amplitude is shown in Figure 2) and *SD*s are also presented in Table S1.

Based on these Taylor diagrams, in general, we do not see any better performance of high-top models over the low-top ones. For negative pattern correlations, the value of the correlation coefficients is below magnitude of 0.2, while the range for positive correction extends up to 0.5 for both the CI and CII regions. More high-top models show a positive correlation than negative correlation in both regions. In the CI region, the better performed models for negative pattern correlations are "J" (CMCC-CESM) and "Y" (GFDL-ESM2G), while in CII region those are "N" (CSIRO-

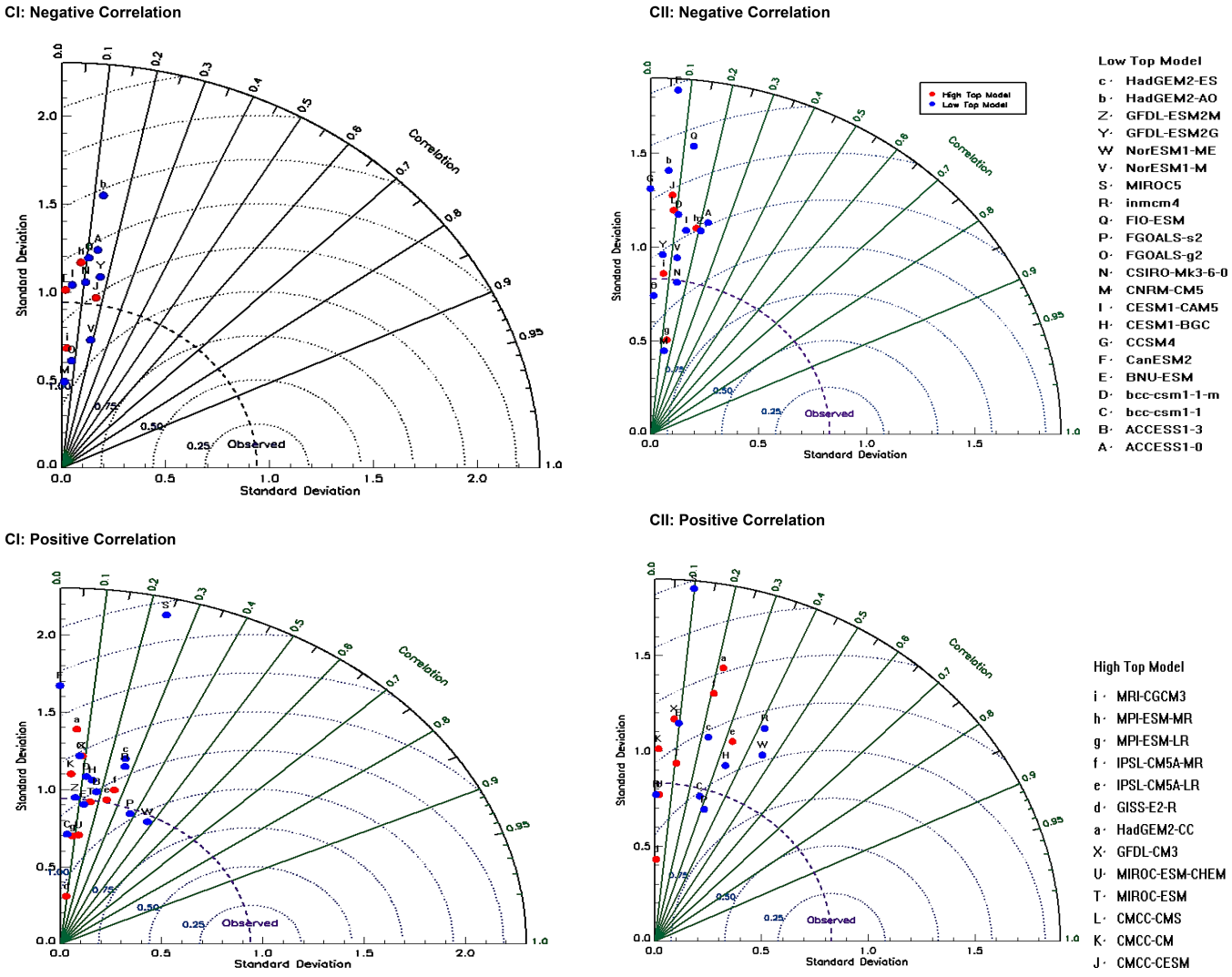

FIGURE 2 Taylor diagram showing pattern correlation (positive and negative) between historical and observational GPCP data in CI and CII region. High-top models are shown by red and low-top ones by blue. Observations are marked by dashed line while RMS errors are shown by dotted lines with magnitudes [Colour figure can be viewed at wileyonlinelibrary.com]

Mk3.6.0) and "V" (NorESM1-M). For positive pattern correlations "P" (FGOALS-s2) and "W" (NorESM1-ME) suggest better in CI region, while "C" (BCC-CSM1.1) and "P" (FGOALS-s2) in CII region. Thus, this diagram indicates model "P" (FGOALS-s2) compares better with observation in terms of mean precipitation and variability for both CI and CII region. Earlier, it was also shown that this model captures regional ISM precipitation variability all over India well (Jourdain *et al*., 2013). We could also identify one high-top model "e" (IPSL-CM5A-LR) that performs better than others. It is also possible to identify poorly performing models; in CI region, for negative pattern correlation, they are "b" (HadGEM2-ES) and for a positive correlation "S" (MIROC5). For CII region, negative correlation, they are "F" (CanESM2) and for a positive correlation, "S." Though it is difficult in general to isolate better performance of high-top models over the low-top ones, however, all the poorly performing models happen to be low-top models in this analysis of the mean state. Model 'S' (MIROC5) is observed as one worst performing models in both CI and CII region.

The similar performance, in general, of high-top and low-top models, seems to be inconsistent with previous results (Charlton-Perez, 2013; Osprey *et al*., 2013; Seviour *et* al., 2016). This is because though stratospheric variability involving the polar vortex may have some role in ISM variability, which effect is overpowered by other strong influences from the troposphere. Those include variation in tropical circulation, moisture convergence from the Indian Ocean, local-scale interactions, etc. We have focussed specific locations from CNE region (CI and CII), which are strongly influenced by both the

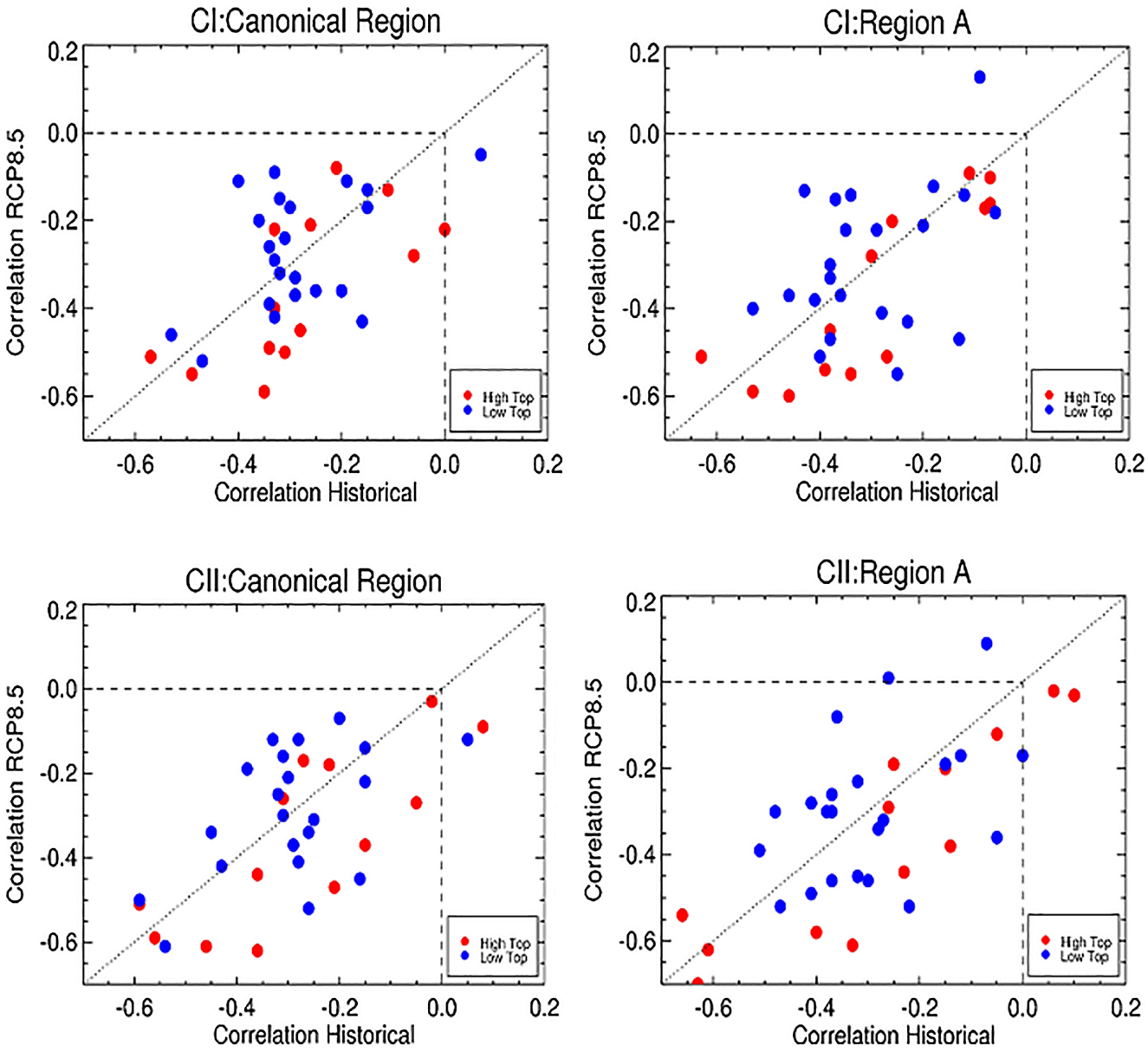

FIGURE 3 Correlation between ISM and SST during historical versus RCP8.5 scenario. SST is chosen in canonical (left) and region A (right) and ISM rainfall is chosen in two different regions CI (top) and CII (bottom). Models showing a negative correlation in both scenarios lie in a box of dashed lines [Colour figure can be viewed at wileyonlinelibrary.com]

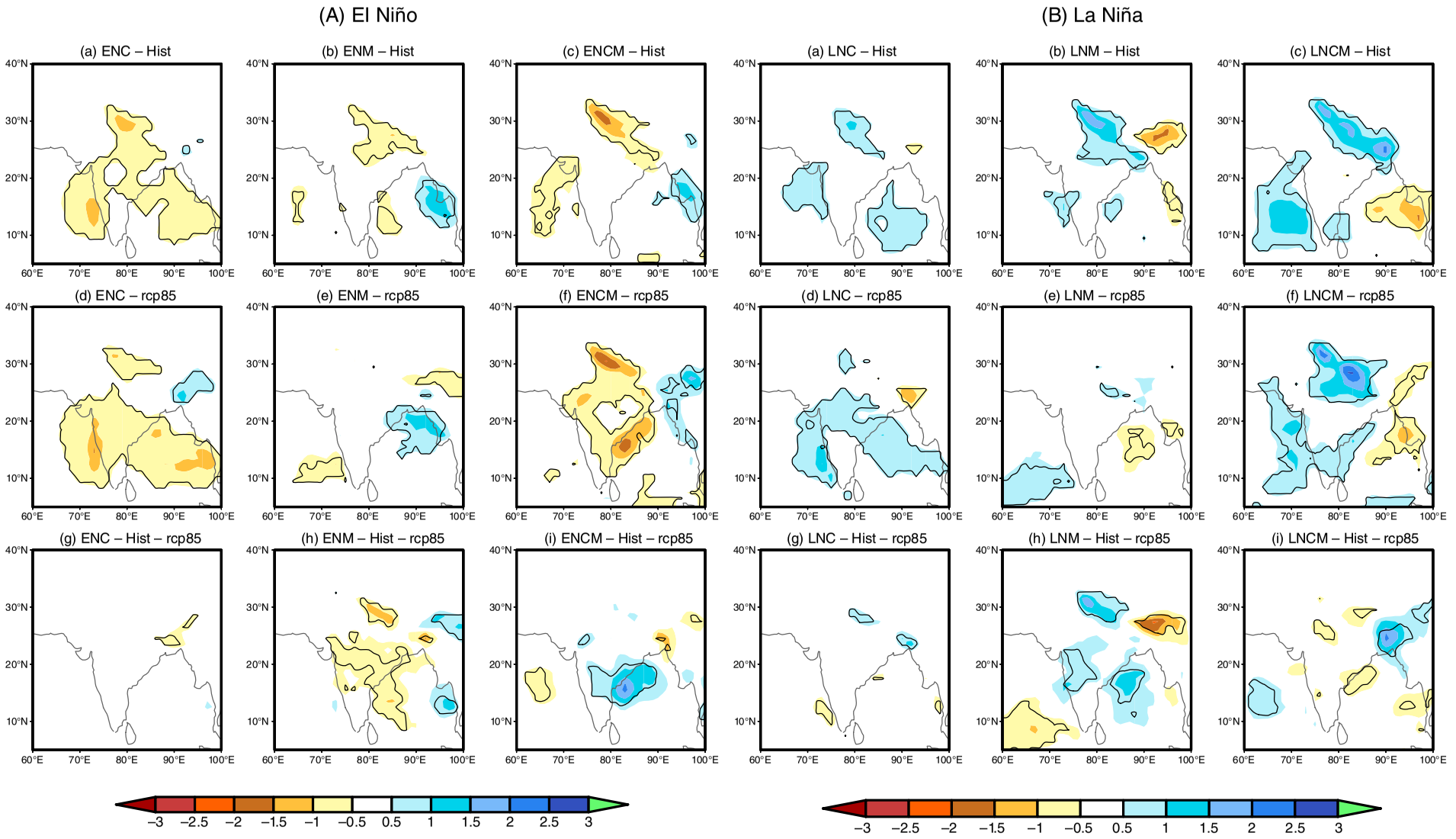

FIGURE 4 The model sub-ensemble mean of ISM composites in historical (a–c), RCP8.5 (d–f) and historical-RCP8.5 scenarios (g–i) are presented in different El Niño (a) and La Niña cases (b). Ensemble mean for various phase of ENSO are shown [El Niño canonical/La Niña canonical (a, d, g), El Niño Modoki/La Niña Modoki (b, e, h) and mixed El Niño canonical-Modoki/La Niña canonical-Modoki (c, f, i)]. Significant regions are outlined with a solid black line [Colour figure can be viewed at wileyonlinelibrary.com]

Hadley and Walker cells. As ISM is influenced by various factors mentioned above, there exists inter-model diversity for both types of models, high or low top.

3.2 | Correlation between ISM and SST in canonical and region A

The correlation coefficients in the historical and RCP scenario between ISM and tropical Pacific SST in regions CI (Figure 3, top) and CII (Figure 3, bottom) show clustering around the one-to-one line, though models show most spread for the CII, region A relationship. A tighter relationship, with lesser spread among models, is apparent when SST in the canonical region are used instead of region A and also for CI instead of CII, respectively (these correlations are relatively insensitive to the choice of SST indices, Figure S1). In Figure S1, we have used Niño4 and Niño3 instead of region A and canonical region, respectively.

Almost all models show negative correlation for the historical and RCP scenarios. For canonical region SSTAs (left), only one model for region CI shows a positive correlation in historical scenario while, for region CII, two models show a positive correlation. For region A (right), one model shows a positive correlation between SSTs and CI under the RCP8.5 scenario and two models show a positive correlation in the historical and RCP8.5 scenario in the CII region. More red points are inclined below the one-to-one line to indicate that, in general, high-top models show a stronger correlation in RCP8.5 than historical scenario. Such association is strongest for CII, region A (Figure 3, bottom right) where only two high-top models lie above the one to one line.

Individual model results for correlations are also presented in Figure S2, where one typical low-top model (CCSM4) is shown alongside one typical high-top model (GISS-E2-R). GISS-E2-R fails to indicate any signal in almost the whole of the country for region A (bottom right). Signals in CCSM4 are in general stronger than that from GISS-E2-R.

As El Niño and La Niña are not opposite mirror images, correlation studies are likely to miss many important teleconnection features in various ENSO phases. Hence, a compositing technique may be more appropriate and are applied in the next section.

3.3 | Model sub-ensemble of ISM composites in the historical and RCP8.5 scenario

The historical precipitation composite from the model sub-ensemble is compared with the RCP8.5 scenario in Figure 4. Models which reproduce the climatology of ISM rainfall over India well (Jourdain *et al*., 2013) are used for ensemble analyses (shown as model number 1–8 in Table S1). A group of eight models are chosen [ACCESS1-0 (1), CCSM4 (2), CanESM2 (3), FIO-ESM (4), HadGEM2-AO (5), HadGEM2-ES (6), MIROC5 (7), NorESM1-ME (8)] (although results are also similar using all models).

For the historical scenario, model sub-ensemble indicates a significant signature of precipitation around the CI region, which is negative for El Niño (Figure 4Aa–c) phase and positive for La Niña (Figure 4Ba–c) in all subcategories. This is discussed in detail in an earlier study (Roy *et al*., 2017), where it was shown that there exists a strong anticorrelation between ISM rainfall and tropical Pacific SST in CI and CII region. This is true for all phases of ENSO: canonical, Modoki or canonical Modoki. CMIP5 models show consistency in capturing the anticorrelation, in agreement with observations. The possible mechanism was discussed in terms of the impact of variations in the Walker circulation.

It is noteworthy that in terms of tropical Pacific SST pattern, CMIP5 models can separate the canonical and Modoki ENSO features reasonably well (Taschetto, 2014; Roy *et al*., 2017; 2018). All models can show some evidence of both modes though some models are better than others. It is also true for the chosen subset of models as used here for ensemble.

Interestingly, when we focus on Figure 4d–f, canonical and canonical Modoki ENSO is shown to be strengthened in some parts in the RCP8.5 scenario, while Modoki ENSO is weakened. For Modoki, practically no signature is detected in land regions (e). For canonical and canonical Modoki case that CII region shows stronger signal in the RCP8.5 scenario, though the CI region is dominant in the historical period. When the variation between the historical and RCP8.5 experiments is considered (Figure 4g–i), it shows major changes for Modoki events (h). The variation is mainly noticed around the CNE region and southern India (h), though stronger in the CNE region. Interestingly, for El Niño, there is a rise in precipitation, while for La Niña a decrease is seen in RCP8.5 scenario when compared to the historical case, which is opposite in nature to that of the usual ISM–ENSO teleconnection. Moreover, around similar locations, a "mirror image" kind of pattern (El Niño vs. La Niña) is noticed for Modoki, in both cases of historical and RCP scenarios, respectively. For the canonical case, the "mirror image" pattern (which reverses in El Niño phase to that from La Niña around CNE region) though present in the historical scenario, but not seen for the RCP situation.

The composite anomaly (historical and RCP) of ISM for two typical individual models (bcc-csm1-1 and NorESM1-ME, those who perform better as noted in Figure 2, are also shown Figure S3).

In subsequent analyses, we discuss mechanisms relating to changes in teleconnection for Modoki for the future scenario with that from a canonical pattern.

3.4 | Addressing dynamical mechanism for the future scenario

Focusing on the meridional and zonal wind at 200 mb level (u200) we explore further the associated dynamical features of ISM–ENSO teleconnections (Figure 5) for the future. Zonal wind figures (left panels) have a stronger influence than meridional winds (right panels). The ensemble mean (black diamond) indicates nearly zero rainfall composite for meridional winds in almost all models. For zonal wind, we observe the majority of models show more rain for La Niña years (second, fourth and sixth row) while less rain during El Niño (first, third and fifth row). This follows the typical ENSO–ISM connection. For canonical ENSO, models indicate consistencies between precipitation and u200, agreeing with a usual negative association. Following the direction of east–west Walker circulation, precipitation is negatively correlated with local zonal eastwards velocity at 200 hPa (first and second row, left). However, for Modoki ENSO and combined canonical and Modoki case, models show large differences and the relationship is not well defined. All these analyses provide a possible explanation why the ISM behaves differently in Modoki years than that from canonical years in RCP scenario as noticed in ensemble mean (Figure 4). A previous paper (Roy *et al*., 2017) discussed the mechanism for this in the historical scenario where canonical, canonical Modoki and Modoki ENSO in CMIP5 models suggested similarly and in all three cases, and u200 played important roles on ISM precipitation.

In RCP scenario, as Figure 4 detected that there is stronger connection for CII region, we presented CII in Figure 5; but the result is also consistent with the CI region (Figure S4) and the S1 region (Figure S5).

In the subsequent section, we discuss results from precipitation decomposition technique, which can separate out contributions from the "thermodynamic" and "dynamic" parts of the changes (Seager *et al*., 2012; Chung *et al*., 2014). Those are also discussed for different flavours of ENSO (Huang *et al*., 2013; Huang, 2014; Huang and Xie, 2015). Similar analysis in the context of South America was most recently performed by Tedeschi and Collins (2017).

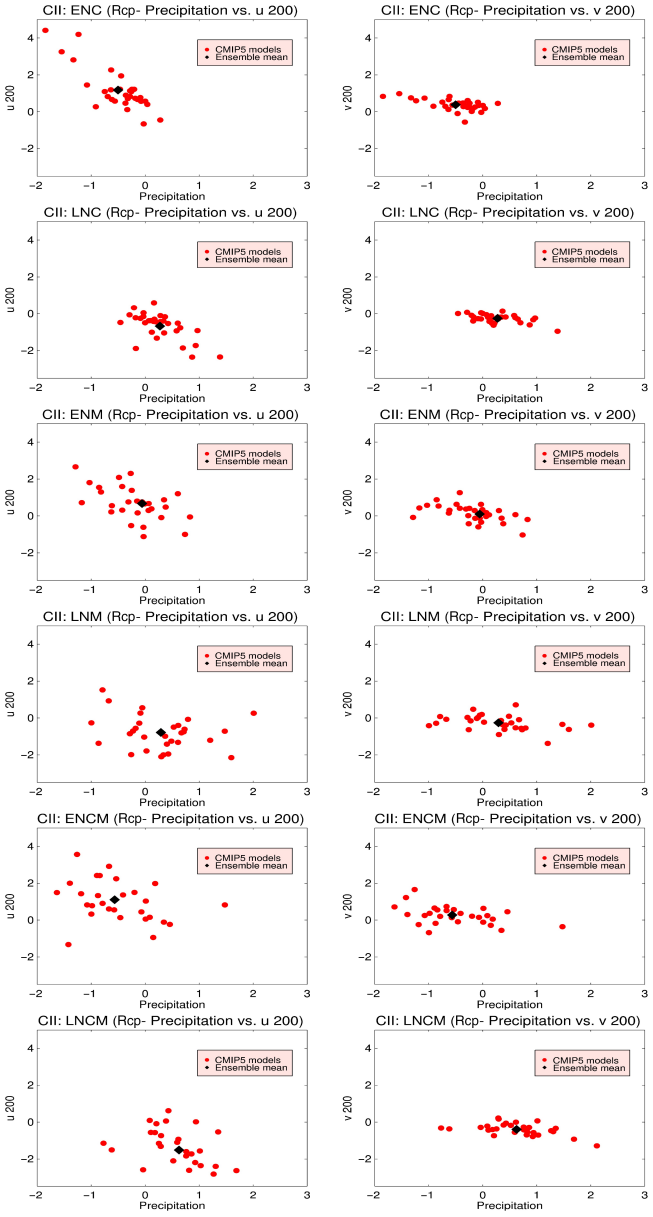

FIGURE 5 ISM precipitation (mm/day) around CII region versus wind 200 (m/s) during JJA in different phases of EN(C/M/CM) and LN(C/M/CM) composites for the future scenario. The top two panels are for canonical phase, the bottom two for combined canonical and Modoki phase, while the middle two (third and fourth panels) for Modoki phase. The left panel is a zonal component of the wind (u), while the right for meridional component (v) [Colour figure can be viewed at wileyonlinelibrary.com]

3.5 | Analyses using the precipitation decomposition technique

Using the decomposition technique, the changes in tropical precipitation under climate change can be examined (Equation 1), where the first part is linked to variations in circulation and the second part to changes in moisture availability (Held and Soden, 2006; Huang *et al*., 2013; Huang, 2014). Using scatter plots, such variations are analysed for the mean climate of the CI, CII, and S1 regions (Figure 6). Region S1 shows a larger spread than that from CI and from CII. The variations of circulation acting on the historical scenario moisture are all negative (first term of Equation 1 and Figure 6, top row), for both CI and CII region, regardless of the precipitation changes. The circulation weakens, reducing that component of the monsoon. The contribution is positive if changes of moisture are considered in combination with wind vertical velocity at 500 hPa from the historical scenario (second term of Equation 1, bottom row). This is true for all eight models and hence also true for the model ensemble mean. The second term dominates, indicating a general increase in mean monsoon rainfall in the future.

In terms of ISM–ENSO teleconnection, the situation is different. Figure 7 suggests the change in precipitation in

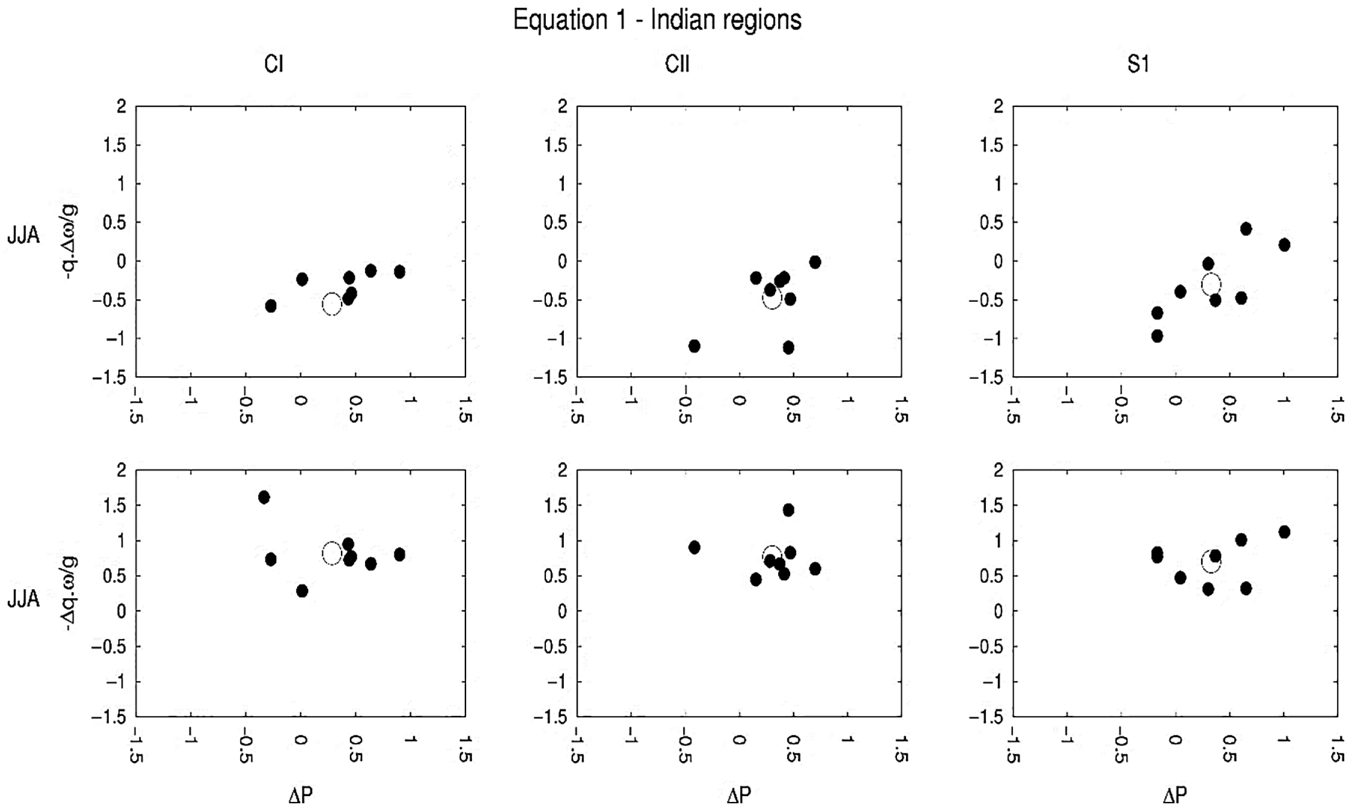

FIGURE 6 Scatter plots of parts of precipitation decomposition Equation 1 versus mean precipitation during JJA in different regions [CI (left), CII (middle) and S1 (right)]. The top row shows the first part of the decomposition precipitation [$(-q\cdot\Delta\omega)$ g^{-1}, mm/day], while bottom row the last part [$-(\Delta q\cdot\omega)$ g^{-1} mm/day]. Circles represent eight chosen CMIP5 models, and open circle represents the ensemble-mean of those models

future around CII region is dominated by the second part of decomposition precipitation, the anomalous circulation multiplied by the climatological moisture, Equation 2 [$(-q\cdot\Delta\omega')$ g^{-1}, mm/day], as shown in the third row. It indicates that the water vapour content in the historical scenario, as well as a change in wind vertical velocity at 500 hPa for particular ENSO phase, both play crucial roles in ISM–ENSO precipitation change. Contributions from the three other terms of Equation 2 are seen to be very small, with the third term being the smallest (Figure 7, fourth row). Modoki ENSOs are particularly more responsive than other modes to the changing scenario. Moreover, the Modoki phase during El Niño shows stronger variation than its La Niña counterpart. Interestingly, Modoki ENSO suggests opposite ENSO–ISM teleconnection, which is shown as a positive change for El Niño years and negative for La Niña. This is captured by most of the models and hence also for the ensemble mean. Such feature is also captured in Figure 4h. A similar observation is noticed when we consider regions CI (Figure S6) and S1 (Figure S7). However, contributions from first [$(-\Delta q\cdot\omega')$ g^{-1}, mm/day] and fourth terms [$(-\Delta q'\cdot\omega)$ g^{-1}, mm/day] from Equation 2 (shown in second and fifth row of the figure) are higher in the CI region to that from CII and S1.

Here are some physical explanations relating to contributions of the dynamic and thermodynamic part on precipitation changes. For the mean climate, the circulation weakens but the increased moisture "wins" and the ISM precipitation goes up. For the ISM–ENSO teleconnection, changes in circulation are most important but these are quite different in different models.

4 | SUMMARY AND CONCLUSION

The teleconnections between the ISM and ENSO are analysed in CMIP5 models. Representative concentration pathways 8.5 simulations (RCP8.5) are compared with the historical period for a subset of models chosen because of their performance in simulating mean ISM rainfall. Techniques of correlation and compositing are applied, focusing on regions of CNE India (CI and CII), as these are the meeting points of regional Hadley and Walker circulations. Different flavours of ENSO are considered. The correlation analyses show that almost all models indicate negative ENSO–ISM correlation for both historical and RCP Scenario, for both canonical and Modoki ENSO variability, with the former showing stronger correlations.

Under the RCP8.5 scenario, the ISM–ENSO teleconnection for canonical and canonical Modoki categories of event is shown to be strengthened. Conversely, for Modoki events, it is weakened. Moreover, for canonical and canonical Modoki, CII region shows a stronger teleconnection in the RCP scenario, while CI shows a more dominant teleconnection in

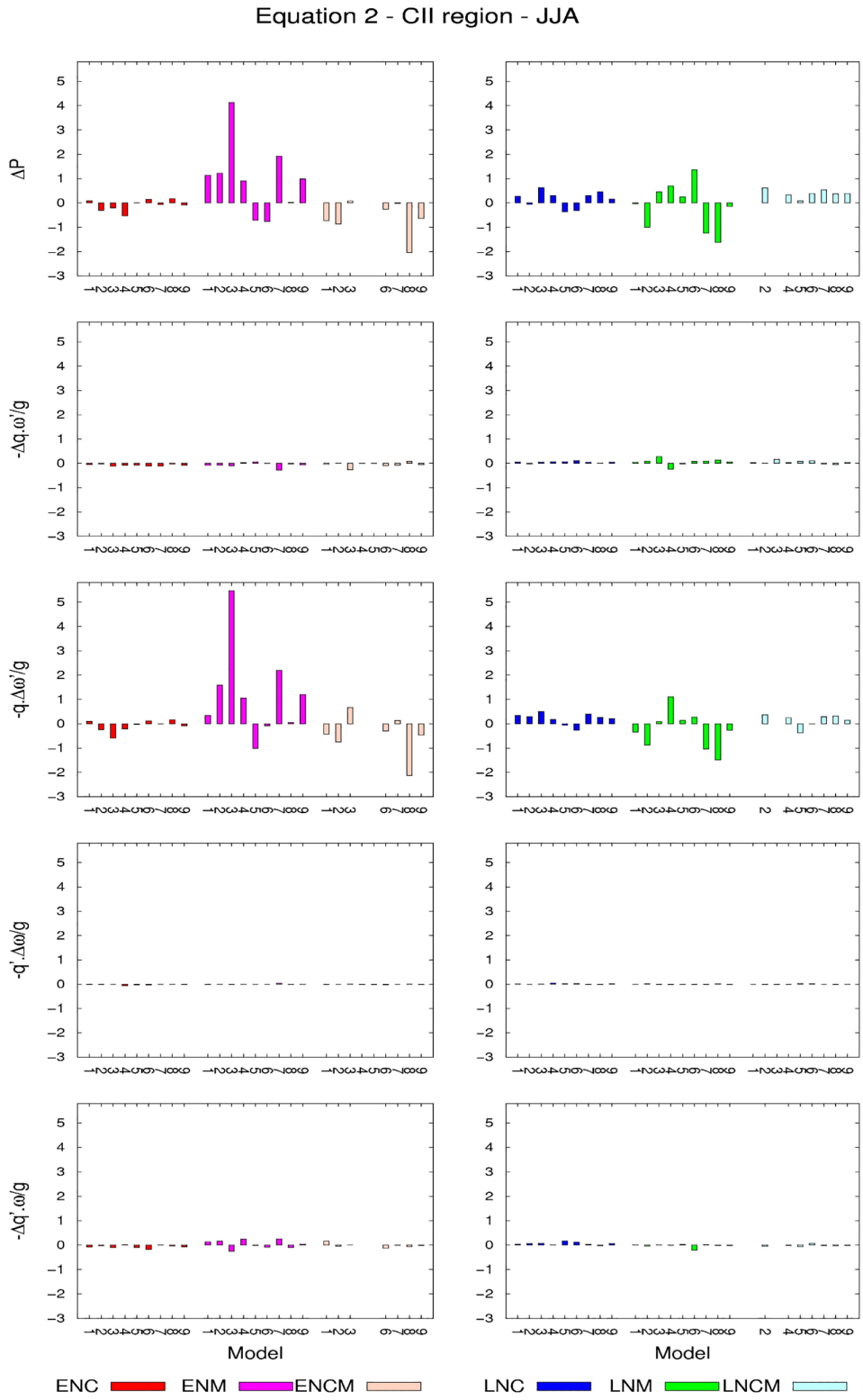

FIGURE 7 Different parts of precipitation decomposition Equation 2 for different ensemble models during JJA in CII region. First row: precipitation (mm/day); second row: first part of decomposition precipitation $[-(\Delta q \cdot \omega')\ g^{-1}$, mm/day]; third row: second part of decomposition precipitation $[(-q \cdot \Delta\omega')\ g^{-1}$, mm/day]; fourth row: third part of decomposition precipitation $[(-q' \cdot \Delta\omega)\ g^{-1}$, mm/day]; and last row: fourth part of decomposition precipitation $[(-\Delta q' \cdot \omega)\ g^{-1}$, mm/day] during El Niño (left column) and La Niña (right column). Numbers (1–8) on the *x*-axis indicate model numbers for the sub-ensemble (marked in Table S1), while number 9 indicates the ensemble mean of all eight models [Colour figure can be viewed at wileyonlinelibrary.com]

the historical case. Modoki ENSO has no influence on Indian land regions in RCP8.5 simulations. The largest variation between models is seen for Modoki ENSO case in the future compared to a historical scenario.

The associated dynamical features of ISM for future are analysed, focusing on the meridional and zonal wind at 200mb level. It is observed that the zonal wind has a stronger influence on rainfall changes while meridional winds are

much less important. For canonical ENSO, models indicate consistencies in terms of Walker circulation, eastwards zonal velocity and precipitation, agreeing with usual ENSO–ISM correlation. But for Modoki and combined canonical Modoki ENSO, there is no consist picture and models show a large deviation in their projections, and hence fail to reveal a clear signal in ensemble mean.

A rainfall decomposition technique reveals a battle between changes in circulation which act to weaken the mean ISM rainfall and changes in moisture change which act to strengthen it. The picture is most consistent in the sub-ensemble of models in the CNE region but less consistent in southern India. It indicates that when the variations of circulation change are combined with water vapour contents from historical scenario it contributes negatively to change in future precipitation. While the contribution is positive and greater if variations of moisture are considered in combination with wind vertical velocity at 500 hPa for historical cases. It is consistent in CI and CII region using all eight ensemble models and results in an increase in mean ISM rainfall.

The precipitation decomposition technique is also applied to analyse the change in ENSO–ISM teleconnection in future for various ENSO phases. It suggests that changes in circulation are most important but without a consistency in the sign of the change. It is also noticed that Modoki events show a greater range of circulation responses than other modes in the RCP8.5 scenario. Moreover, El Niño Modoki shows stronger variation to that from its La Niña counterparts.

Overall, using CMIP5 model simulations and analysing future projections, this study indicates the nature of ISM precipitation and ENSO–ISM teleconnection in a changing climate. Such knowledge would be highly beneficial for future planning purposes.

ACKNOWLEDGEMENTS

MC acknowledges funding from NERC, funding number NE/I022841/1.

ORCID

Indrani Roy https://orcid.org/0000-0003-1728-7506
Renata G. Tedeschi https://orcid.org/0000-0002-9312-0030
Matthew Collins https://orcid.org/0000-0003-3785-6008

REFERENCES

Ashok, K., Guan, Z. and Yamagata, T. (2001) Impact of Indian Ocean dipole on the relationship between the Indian monsoon rainfall and ENSO. *Geophysical Research Letters*, 28(23), 4499–4502.

Ashok, K., Behera, S.K., Rao, S.A., Weng, H. and Yamagata, T. (2007) El Niño Modoki and its possible teleconnection. *Journal of Geophysical Research*, 112, C11007. https://doi.org/10.1029/2006JC003798.

Azad, S. and Rajeevan, M. (2016) Possible shift in the ENSO–Indian monsoon rainfall relationship under future global warming. *Scientific Reports*, 6, 20145.

Bollasina, M.A., Ming, Y. and Ramaswamy, V. (2011) Anthropogenic aerosols and the weakening of the South Asian summer monsoon. *Science*, 334, 502–505. https://doi.org/10.1126/science.1204994.

Brown, J.N., McIntosh, P.C., Pook, M.J. and Risbey, J.S. (2009) An investigation of the links between ENSO flavors and rainfall processes in southeastern Australia. *Monthly Weather Review*, 137, 3786–3795.

Cai, W. and Cowan, T. (2009) La Niña Modoki impacts Australia autumn rainfall variability. *Geophysical Research Letter*, 36, L12805. https://doi.org/10.1029/2009GL037885.

Cai, W., Santoso, A., Wang, W., Yeh, S.-W., An, S.-I., Cobb, K.M., Collins, M., Guilyardi, E., Jin, F.-F., Kug, J.-S., Lengaigne, M., McPhaden, M.J., Takahashi, K., Timmermann, A., Vecchi, G., Watanabe, M. and Wu, L. (2015) ENSO and greenhouse warming. *Nature Climate Change*, 5, 849–859.

Cappondonti, A., Wittenberg, A.T., Newman, M., Lorenzo, E.D., Yu, J.-Y., Braconnot, P., Cole, J., Dewitte, B., Giese, B., Guilyardi, E., Jin, F.-F., Karnnauskas, K., Kirtman, K., Lee, T., Schneider, N., Xue, Y. and Yeh, S.-W (2015) Understanding ENSO diversity. *Bulletin of the American Meteorological Society*, 96, 921–938. https://doi.org/10.1175/BAMS-D-13-00117.1.

Chadwick, R., Boutle, I. and Martin, G. (2013) Spatial patterns of precipitation change in CMIP5: why the rich do not get richer in the tropics. *Journal of Climate*, 26, 3804–3822. https://doi.org/10.1175/JCLI-D-12-00543.1.

Charlton-Perez, A.J. (2013) On the lack of stratospheric dynamical variability in low-top versions of the CMIP5 models. *Journal of Geophysical Research: Atmosphere*, 118(6), 2494–2505. https://doi.org/10.1002/jgrd.50125.

Chou, C., Neelin, J., Chen, C. and Tu, J. (2009) Evaluating the "rich-get-richer" mechanism in tropical precipitation change under global warming. *Journal of Climate*, 22, 1982–2005.

Chung, C.T.Y., Power, S.B., Arblaster, J.M., Rashid, H.A. and Roff, G.L. (2014) Nonlinear precipitation response to El Niño and global warming in the Indo-Pacific. *Climate Dynamics*, 42, 1837–1856. https://doi.org/10.1007/s00382-013-1892-8.

Gill, A.E. (1980) Some simple solutions of heat induced tropical circulations. *Quarterly Journal of the Royal Meteorological Society*, 106, 447–462.

Goswami, B.N., Venugopal, V., Sengupta, D., Madhusoodanan, M.S. and Xavier, P.K. (2006) Increasing trend of extreme rain events over India in a warming environment. *Science*, 314, 1442–1445.

Grimm, A.M. (2004) How do La Niña events disturb the summer monsoon system in Brazil? *Climate Dynamics*, 22, 123–138.

Held, I.M. and Soden, B.J. (2006) Robust responses of the hydrological cycle to global warming. *Journal of Climate*, 19, 5686–5699.

Huang, P. (2014) Regional response of annual-mean tropical rainfall to global warming. *Atmospheric Science Letters*, 15, 103–109. https://doi.org/10.1002/asl2.475.

Huang, P. and Xie, S.-P. (2015) Mechanisms of change in ENSO-induced tropical Pacific rainfall variability in a warming climate. *Nature Geoscience*, 8, 922–926. https://doi.org/10.1038/ngeo2571.

Huang, P., Xie, S.P., Hu, K., Huang, G. and Huang, R. (2013) Patterns of the seasonal response of tropical rainfall to global warming. *Nature Geoscience*, 6, 357–361.

Huffman, G.J., Adler, R.F., Bolvin, D.T. and Gu, G. (2009) Improving the global precipitation record: GPCP version 2.1. *Geophysical Research Letters*, 36, L17808. https://doi.org/10.1029/2009GL040000.

Hurwitz, M.M., Calvo, N., Garfinkel, C.I., Butler, A.H., Ineson, S., Cagnazzo, C., Manzini, E. and Peña-Ortiz, C. (2014) Extra-tropical atmospheric response to ENSO in the CMIP5 models. *Climate Dynamics*, 43, 3367–3376. https://doi.org/10.1007/s00382-014-2110-z.

John, O., Allan, R.P. and Soden, J. (2009) How robust are observed and simulated precipitation responses to tropical ocean warming? *Geophysical Research Letters*, 36, L14702.

Jourdain, N.C., Sen Gupta, A., Taschetto, A.S., Ummenhofer, C.C., Moise, A.F. and Ashok, K. (2013) The Indo-Australian monsoon and its relationship to ENSO and IOD in reanalysis data and the CMIP3/CMIP5 simulations. *Climate Dynamics*, 41, 3073–3102. https://doi.org/10.1007/s00382-013-1676-1.

Kao, H.-Y. and Yu, J.-Y. (2009) Contrasting eastern-Pacific and central-Pacific types of El Niño. *Journal of Climate*, 22, 615–632.

Kug, J.-S., Jin, F.-F. and An, S.-I. (2009) Two types of El Niño events: cold tongue El Niño and warm pool El Niño. *Journal of Climate*, 22, 1499–1515.

Kumar, K.K., Rajagopalan, B., Hoerling, M., Bates, G. and Cane, M. (2006) Unraveling the mystery of Indian monsoon failure during El Niño. *Science*, 314, 115–119.

Lin, H. and Wu, Z. (2012) Indian summer monsoon influence on the climate in the North Atlantic–European region. *Climate Dynamics*, 39, 303–311.

Liu, X. and Yanai, M. (2001) Relationship between the Indian monsoon rainfall and the tropospheric temperature over the Eurasian continent. *Quarterly Journal of the Royal Meteorological Society*, 127, 909–937.

Meyer, P.L. (1970) *Introductory Probability and Statistical Applications*. Reading: Addison-Wesley.

Osprey, S.M., Gray, L.J., Hardiman, S.C., Butchart, N. and Hinton, T.J. (2013) Stratospheric variability in twentieth-century CMIP5 simulations of the Met Office climate model: high top versus low top. *Journal of Climate*, 26, 1595–1606.

Prabhu, A., Kripalani, R.H., Preethi, B. and Pandithurai, G. (2016) Potential role of the February–March Southern Annular Mode on the Indian summer monsoon rainfall: a new perspective. *Climate Dynamics*, 47(3), 1161–1179.

Rayner, N.A., Parker, D.E., Horton, E.B., Folland, C.K., Alexander, L.V., Rowell, D.P., Kent, E.C. and Kaplan, A. (2003) Global analyses of sea surface temperature, sea ice, and night marine air temperature since the late nineteenth century. *Journal of the Geophysical Research*, 108(D14), 4407. https://doi.org/10.1029/2002JD002670.

Riahi, K., Rao, S., Krey, V., Cho, C., Chirkov, V., Fischer, G., Kindermann, G., Nakicenovic, N. and Rafaj, P. (2011) RCP-8.5—a scenario of comparatively high greenhouse gas emission. *Climate Change*, 109, 33–57. https://doi.org/10.1007/s10584-011-0149-y.

Ropelewski, C.F. and Halpert, M.S. (1987) Global and regional scale precipitation patterns associated with the El Niño–Southern Oscillation. *Monthly Weather Review*, 115, 1606–1626.

Roy, I. (2017) Indian summer monsoon and El Niño–Southern Oscillation in CMIP5 models: a few areas of agreement and disagreement. *Atmosphere*, 8 (8), 154. https://doi.org/10.3390/atmos8080154.

Roy, I. (2018) *Climate Variability and Sunspot Activity—Analysis of the Solar Influence on Climate*, 1st edition. Basel: Springer Nature, 218 pp.

Roy, I. and Collins, M. (2015) On identifying the role of sun and the El Niño–Southern Oscillation on Indian summer monsoon rainfall. *Atmospheric Science Letters*, 16, 162–169. https://doi.org/10.1002/asl2.547.

Roy, I. and Kriplani, R. (2018) The role of natural factors (part 1): addressing on mechanism of different types of ENSO, related teleconnections and solar influence. *Theoretical and Applied Climatology*, 1–12. https://doi.org/10.1007/s00704-018-2597-z.

Roy, I. and Tedeschi, R.G. (2016) Influence of ENSO on regional ISM precipitation–local atmospheric influences or remote influence from Pacific. *Atmosphere*, 7, 25. https://doi.org/10.3390/atmos7020025.

Roy, I., Tedeschi, R.G. and Collins, M. (2017) ENSO teleconnections to the Indian summer monsoon in observations and models. *International Journal of Climatology*, 37, 1794–1813. https://doi.org/10.1002/joc.4811.

Roy, I., Gagnon, A.S. and Singh, D. (2018) Evaluating ENSO teleconnections using observations and CMIP5 models. *Theoretical and Applied Climatology*, 1–14. https://doi.org/10.1007/s00704-018-2536-z.

Seager, R., Naik, N. and Vecchi, G.A. (2010) Thermodynamic and dynamic mechanisms for large-scale changes in the hydrological cycle in response to global warming. *Journal of Climate*, 23, 4651–4668. https://doi.org/10.1175/2010JCLI3655.1.

Seager, R., Naik, N. and Vogel, L. (2012) Does global warming cause intensified interannual hydroclimate variability? *Journal of Climate*, 25, 3355–3372. https://doi.org/10.1175/JCLI-D-11-00363.1.

Seviour, W.J.M., Gray, L.J. and Mitchell, D.M. (2016) Stratospheric polar vortex splits and displacements in the high-top CMIP5 climate models. *Journal of Geophysical Research: Atmospheres*, 121(4), 1400–1413.

Taschetto, A.S. (2014) Cold tongue and warm pool ENSO events in CMIP5: mean state and future projections. *Journal of Climate*, 27, 2861–2855. https://doi.org/10.1175/JCLI-D-13-00437.1.

Taylor, K.E. (2001) Summarizing multiple aspects of model performance in a single diagram. *Journal of Geophysical Research: Atmospheres*. Washington, DC: American Geophysical Union. Available at: http://wwwpcmdillnl.gov/publications/ab55.html [Accessed 1st April 2011].

Taylor, K.E., Stouffer, R.J. and Meehl, G.A. (2012) An overview of CMIP5 and the experimental design. *Bulletin of the American Meteorological Society*, 93, 485–498. https://doi.org/10.1175/BAMS-D-11-00094.1.

Tedeschi, R.G. and Collins, M. (2017) The influence of ENSO on South American precipitation: simulation and projection in CMIP5 models. *International Journal of Climatology*, 37, 3319–3339. https://doi.org/10.1002/joc.4919.

Tedeschi, R.G., Cavalcanti, I.F.A. and Grimm, A.M. (2013) Influences of two types of ENSO on South American precipitation. *International Journal of Climatology*, 33, 1382–1400. https://doi.org/10.1002/joc.3519.

Turner, A.G., Inness, P.M. and Slingo, J.M. (2005) The role of the basic state in the ENSO–monsoon relationship and implications for predictability. *Quarterly Journal of the Royal Meteorological Society*, 131(607), 781–804.

Wang, B., Liu, J., Kim, H.J., Webster, P.J., Yim, S.Y. and Xiang, B.Q. (2013) Northern Hemisphere summer monsoon intensified by mega-El Niño/Southern Oscillation and Atlantic multidecadal oscillation. *Proceedings of the National Academy of Sciences of the United States of America*, 110(14), 5347–5352.

Wu, Z. and Zhang, P. (2015) Interdecadal variability of the mega-ENSO–NAO synchronization in winter. *Climate Dynamics*, 45, 1117–1128. https://doi.org/10.1007/s00382-014-2361-8.

Xie, S.P., Deser, C., Vecchi, G.A., Ma, J., Teng, H. and Wittenberg, A.T. (2010) Global warming pattern formation: sea surface temperature and rainfall. *Journal of Climate*, 23, 966–986.

Yeh, S.W., Cai, W., Min, S.-K., McPhaden, M.J., Dommenget, D., Dewitte, B., Collins, M., Ashok, K., An, S.-I., Yim, B.-Y. and Kug, J.-S. (2018) ENSO atmospheric teleconnections and their response to greenhouse gas forcing. *Review of Geophysics*, 56, 185–206. https://doi.org/10.1002/2017RG00568.

Yu, J.-Y. and Kim, S.T. (2011) Relationships between extratropical sea level pressure variations and the central-Pacific and eastern-Pacific types of ENSO. *Journal of Climate*, 24, 708–720.

Zhang, L., Wu, Z. and YF, Z. (2016) Different impacts of typical and atypical ENSO on the Indian summer rainfall: ENSO-developing phase. *Atmosphere-Ocean*, 54, 440–456.

Zhang, P., Wu, Z. and Chen, H. (2017) Interdecadal variability of the ENSO–North Pacific atmospheric circulation in winter. *Atmosphere-Ocean*, 55, 110–120. https://doi.org/10.1080/07055900.2017.1291411.

Zou, L. and Zhou, T. (2015) Asian summer monsoon onset in simulations and CMIP5 projections using four Chinese climate models. *Advances in Atmospheric Sciences*, 32, 794–806. https://doi.org/10.1007/s00376-014-4053-z.

SUPPORTING INFORMATION

Additional supporting information may be found online in the Supporting Information section at the end of the article.

How to cite this article: Roy I, Tedeschi RG, Collins M. ENSO teleconnections to the Indian summer monsoon under changing climate. *Int J Climatol*. 2019;1–12. https://doi.org/10.1002/joc.5999